

Analysis of Fiber Bragg Gratings for Dispersion Compensation in Reflective and Transmissive Geometries

Natalia M. Litchinitser and David B. Patterson, *Member, IEEE*

Abstract—Numerical analysis of the dispersion-compensating properties of fiber Bragg gratings (FBG's) in both reflective and transmissive modes is presented. First, the sensitivity of chirped, reflective gratings to the grating chirp parameter, index modulation, and grating length is examined, showing that apodization provides lower sensitivity to variations in these parameters. Second, we introduce a new transmissive geometry for grating-based dispersion compensation that utilizes the dispersive properties of a uniform Bragg grating in transmission.

Index Terms—Compensation, gratings, optical fiber dispersion, optical pulse compression.

I. INTRODUCTION

OPTICAL fiber Bragg gratings (FBG's) have recently been shown to have practical application in compensation of dispersion-broadening in long-haul communication. While Lam *et al.* first discussed the use of unchirped gratings for compensation, a subsequent landmark paper by Ouellette first described the use of chirped reflection gratings to provide frequency-dependent delays for recompression of dispersed pulses [1]–[3]. Subsequently, several groups have developed systems employing these dispersion compensators, showing that gratings of only a few centimeters length are capable of nearly full compensation of the dispersion induced by propagation in hundreds of kilometers of fiber [4]–[7]. While these experimental groups have used a variety of grating profiles, coupling strengths, and grating lengths, the literature is currently lacking a complete analysis of the optimization of the grating parameters and sensitivity of the degree of compensation on these parameters, although some limited optimization work has been reported [8]. As a primary purpose of the present paper, we provide a complete set of optimization curves for a typical reflective grating parameters, including discussion of a tapered profile for decreased sensitivity to grating imperfections. We also find good agreement with the predicted optimization conditions of [2].

As a secondary purpose of our paper, we shall revisit a previously discarded geometry for grating-induced dispersion

compensation via transmission through a uniform grating. While reflective systems have been shown to offer nearly complete compensation, they require insertion of directional couplers or circulators to extract the reflected, recompressed pulse. Thus these systems introduce typical insertion losses in the range of 2–6 dB. A more attractive solution would be a transmission-based system, in which dispersion-compensating gratings could be placed in line with the fiber, perhaps written during fiber fabrication.

In 1990, Ouellette examined the practicality of transmission-based systems, concluding that only a trivially small amount of compensation could be achieved in transmission, as one would be required to use a pulse bandwidth within the narrow sidelobe minimum of the reflectivity spectrum of the Bragg grating [9]. Recently, Eggleton *et al.* have shown that better performance is possible by apodizing the grating, achieving some degree of pulse recompression with a linearly tapered, unchirped grating [10]. In this paper, we introduce a new transmission geometry based on propagation through a uniform, unchirped Bragg grating. Here, we employ a pulse spectrum detuned to the sidelobe region of the grating stop-band with a pulse bandwidth much greater than the spectral width of an individual sidelobe of the grating transmission function. We limit our simulations to relatively weak, short gratings and show that significant dispersion compensation may be achieved with insertion losses rivaling those obtained in the more complicated reflection-based structures. While our constraints on grating parameters do not allow for the optimization of dispersion compensation, these issues are addressed in a subsequent paper found elsewhere in this issue [11].

We begin with a brief review of the reflective Bragg grating geometry, using the theoretical techniques of Kogelnik to develop the reflectivity relations for the chirped grating [12]. We then perform a sequence of two-parameter optimizations, using the recompressed pulse width and intensity as figures of merit for the grating geometry. We analyze the effects of chirp parameter, coupling strength, interaction length, and apodization on these measures, establishing regions of best performance for grating design. We also show that proper tapers in the grating profile provide greater immunity of the compensator to imperfections induced by writing-beam variation by reducing sensitivity to the grating coupling coefficient.

Next, we use the well-known transmission function for the uniform Bragg grating to show that this grating is capable of

Manuscript received October 30, 1996; revised May 5, 1997. This work was supported by the Aileen S. Andrew Foundation.

N. M. Litchinitser was with the Electrical and Computer Engineering Department, Illinois Institute of Technology, Chicago, IL 60616 USA. She is now with the Institute of Optics, University of Rochester, Rochester, NY 14627 USA.

D. B. Patterson is with the Electrical and Computer Engineering Department, Illinois Institute of Technology, Chicago, IL 60616 USA.

Publisher Item Identifier S 0733-8724(97)05923-9.

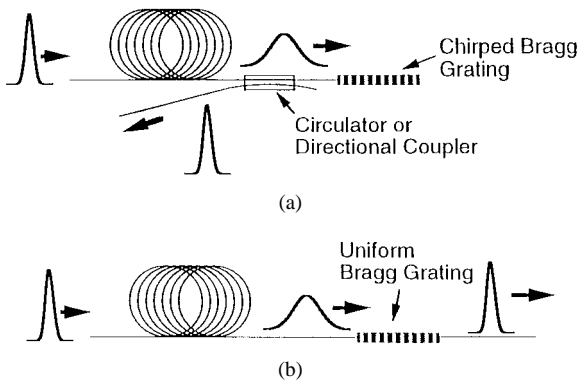


Fig. 1. Schematic system model to investigate dispersion compensation with the fiber Bragg grating in (a) reflective geometry and in (b) transmission geometry.

providing a degree of dispersion compensation that far exceeds the prediction of [9]. We consider a 40-ps full-width at half maximum (FWHM) Gaussian pulse at 1.55 μm wavelength, chirped by propagation through a 100-km length of fiber, that is incident on a uniform Bragg grating. By detuning the center frequency of the dispersion broadened pulse from the resonant frequency of the grating, a combination of grating-induced dispersion and pulse truncation leads to recompression by factors of 2.4, with over 40% of the peak intensity of the undispersed pulse transmitted through the grating.

II. REFLECTIVE BRAGG GRATING COMPENSATORS

The theoretical model used to investigate dispersion compensation with the fiber Bragg grating is shown in Fig. 1(a). The chirped 144 ps (FWHM) pulse is obtained by simulating the transmission of a 40 ps (FWHM) pulse through 100 km of fiber with a dispersion parameter $d^2\beta/d\omega^2$ of $-20 \text{ ps}^2/\text{km}$ at a wavelength of 1.55 μm , followed by a linearly chirped Bragg grating for which the grating parameters are varied.

Consider a waveguide propagating a single mode in the forward and backward direction and suppose that a sinusoidal refractive index perturbation is induced in the waveguide in the form

$$n(z) = n_0 + \Delta n(z) \cos[Kz + \phi(z)] \quad (1)$$

where the refractive index perturbation $\Delta n(z)$ and the phase shift $\phi(z)$ are slowly varying functions of z . The grating spatial frequency $K = 2\pi/\Lambda$ satisfies the Bragg condition $K = 2\beta_0$ where β_0 is the propagation constant of the waveguide mode and Λ is the grating period.

The coupling induced between these modes by the grating function may be described by the well-known coupled-mode equations [2]. Here, we follow the development of [12] solving numerically for the reflection coefficient using the Runge-Kutta method.

We assume that the Bragg grating introduces a coupling coefficient between counterpropagating modes with amplitude variation

$$\kappa(z) = \kappa_0 \exp\{-Az^2\} \quad (2)$$

where κ_0 is a constant normalized coupling coefficient and A provides a Gaussian taper over the grating ($-0.5 \leq z \leq 0.5$).

Implicit is the assumption that the grating also contains a linearly chirped phase function $\phi(z) = (F/2)(z^2/L_g^2)$ where parameter F is a measure of the amount of the chirp and L_g is the length of the grating. We solve for the reflected pulse width, defining the figures of merit for the grating performance to be pulse compression ratio τ_1/τ_2 (where τ_1 is the pulse width before its passing through the grating, and τ_2 is that after the grating), and peak reflected intensity, limited by the input transform-limited pulse to 3.6 and 1, respectively.

We begin with the Riccati differential equation for the reflection coefficient as a function of position in the grating [12]

$$\rho' = j(2\delta - \phi')\rho + j\kappa_L(1 + \rho^2) \quad (3)$$

where the prime denotes differentiation with respect to position z along the grating, where z is normalized to the grating length L_g ; this makes the solution dimensionless and scalable. The term δ represents the dimensionless detuning of the propagation constant from the resonant propagation constant for the grating, $\beta_0 L_g$, while κ_L represents the dimensionless coupling coefficient, κL_g . The differential equation is then solved over the dimensionless range $|z| \leq 0.5$.

Following the approach of [12], (3) must be solved numerically in the case of the linear chirp function defined above. We solve for the reflection coefficient spectrum using the Runge-Kutta technique, and the reflected pulse is reconstructed from its frequency components, with the peak intensity and pulse FWHM determined.

We performed the analysis under variations of the parameters F , L_g , κ , and A , by fixing one of the three variables and mapping the results of the other two. (The fixed value was determined to be near optimum through iterations of the technique.) In Fig. 2, we plot the compression and the intensity contours as functions of the grating length L_g and the parameter F/L_g , with the coupling coefficient κ fixed at $0.675\pi \text{ cm}^{-1}$. By varying L_g and F/L_g , we simulate a single chirped phase mask which is exposed over various lengths to form the grating; thus, the range variation of the resonant spatial frequency is changed. (A plot with varying F and L_g would be equivalent to examining different phase masks that spanned the same spatial frequency range despite their different lengths, i.e., the physical chirp of the mask must be changed each time.)

From Fig. 2, we observe regions where the grating provides nearly perfect compensation, approaching the compression limit of 3.60 and the intensity limit of 1.00. We may compare this result with the predicted optimal values of [2]. Here the chirped grating was modeled as a continuum of point reflectors, each reflecting the resonant optical wavelength corresponding to twice the local grating period. This simple model produces frequency-dependent time delays in the reflected pulse, and thus provides dispersion compensation. Using this argument, the relationship between chirp parameter F and grating length L_g is found to be [2]

$$L_g^2 = \frac{c^2 \beta_2 L_f}{4n_0^2} F \quad (4)$$

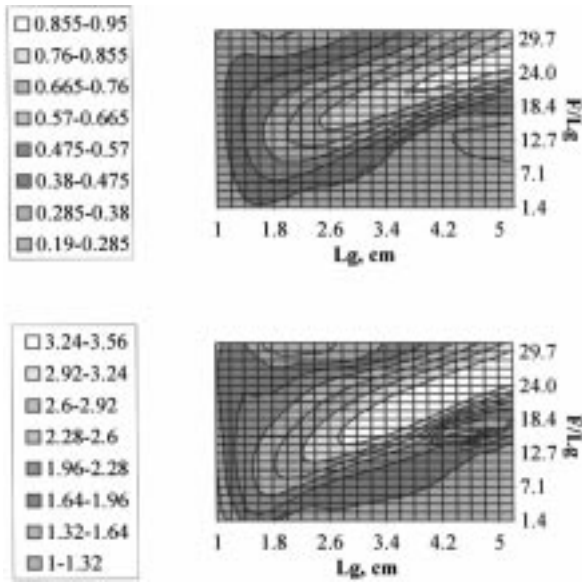


Fig. 2. The peak intensity and compression ratio as functions of the grating length L_g and the parameter F/L_g , with the coupling coefficient κ fixed at $0.675\pi \text{ cm}^{-1}$.

where c is the speed of light $\beta_2 = d^2\beta/d\omega^2$ is the dispersion parameter and L_f is the length of the dispersive fiber, and n_0 is the effective index of the fiber mode.

Using this model, (4) predicts a slope of the optimum region in the L_g versus F/L_g graph to be 0.212 cm^2 . From the graph, we see a slope of 0.217 cm^2 , showing good agreement with Ouellette's theoretical analysis [2].

In Fig. 3, we fix the grating length $L_g = 4 \text{ cm}$ and plot the compression and intensity contours versus the chirp parameter F/L_g and the coupling-length product, $\kappa L_g/\pi$. We see that the results are most sensitive to the chirp parameter. For moderate coupling strengths, the optimum compression occurs at a constant value of F/L_g ; however, as the coupling strength is increased, the optimum region tends to move toward regions of greater chirp. This result also shows that the compensator performance will degrade with large overcoupling for a fixed chirp parameter.

This degradation may be eliminated by introducing a taper into the grating. It is well known that apodization of Bragg gratings eliminates sidelobes in the reflectance spectrum and in the grating dispersion function [2]. However, the results of Fig. 4 illustrate another use of the tapered grating—maintaining optimum performance for overcoupled gratings. Here, we used a 4-cm grating with a fixed chirp parameter of $F = 26\pi$, and adjust the Gaussian taper parameter A of (2) and the coupling coefficient κ . We observe that the compression and the peak intensity remain in the optimum region as the coupling strength is increased (at fixed F), contrary to the results of Fig. 3 for an untapered grating. We also note that the maximum value obtained in the intensity plot is increased, indicating better performance of the compensator. Hence, the tapered grating will perform well over a broad range of coupling strengths and will lead to better reconstruction of the original pulse. The former conclusion is illustrated in Fig. 5, which is the equivalent of Fig. 3 for an

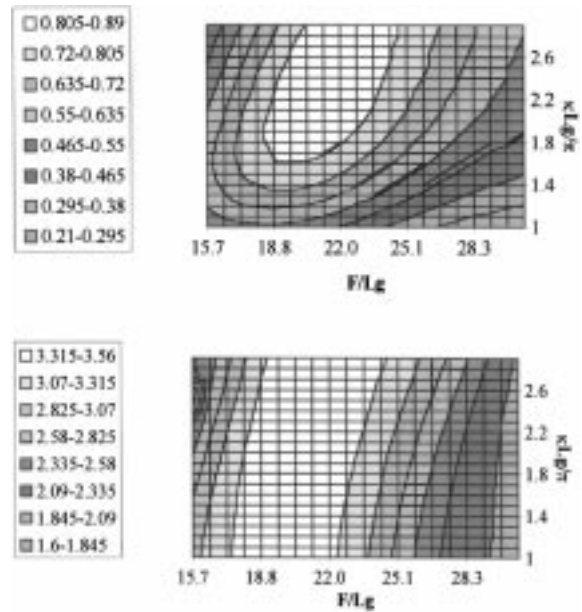


Fig. 3. The peak intensity and compression ratio as functions of the chirp parameter F/L_g and the coupling-length product, $\kappa L_g/\pi$, with the grating length L_g fixed at 4 cm .

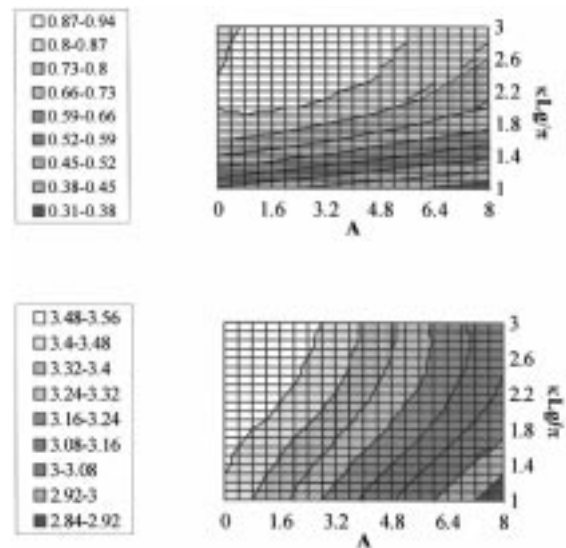


Fig. 4. The peak intensity and compression ratio as functions of the coupling-length product $\kappa L_g/\pi$ and the taper parameter A with a fixed chirp parameter of $F = 26\pi$ and the grating length $L_g = 4 \text{ cm}$.

apodized grating with $A = 3.0$. It is clear that the optimum compression and intensity of the reflected pulse remain at a fixed chirp parameter as the coupling strength is increased. We also note that cross-sectional curves for fixed taper will be flat in this case, with little sensitivity to variations in coupling coefficient κ .

The implications of this result should be of importance to grating compensator designers. Since refractive index modulation depth is a function of the exposure time in basic fabrication techniques, the obtained results suggest that efficient recompression may be obtained over a wide range of grating exposure conditions by introducing an appropriate taper.

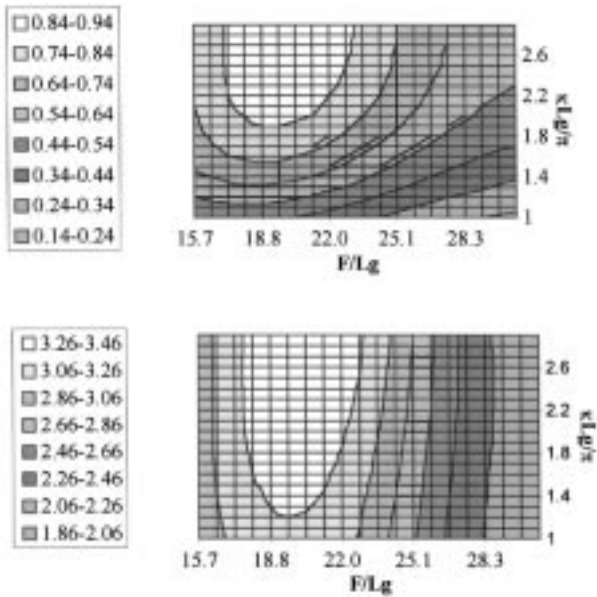


Fig. 5. The peak intensity and compression ratio for an apodized grating with $A = 3.0$ as functions of the chirp parameter F/L_g and the coupling-length product, $\kappa L_g/\pi$, with the grating length L_g fixed at 4 cm.

III. UNIFORM TRANSMISSION GRATINGS

We now consider the transmission through a uniform, unchirped grating. As we stated in Section I, all analyses of this type of grating to date have assumed that the spectral width of the optical pulse must lie within a side peak of the transmission curve for such a grating or that the sidelobe structure must be smoothed by apodization [9], [10]. However, as we show in this section, far better performance is obtained using a broad spectrum, allowing partial reflection of the pulse by the grating.

Our system model is that of Fig. 1(b), where we now consider a uniform (unchirped) grating and examine the transmitted field. Again, we assume that a Gaussian pulse is launched into a length L_f of fiber with propagation constant β_0 , group velocity $1/\beta_1$, and dispersion parameter β_2 , such that the propagation constant is approximated by

$$\beta(\omega) = \beta_0 + \beta_1(\omega - \omega_0) + \frac{1}{2}\beta_2(\omega - \omega_0)^2, \quad (5)$$

The input electric field has the form

$$E_{in}(t) = \exp\left\{-\frac{1}{2}\left(\frac{t}{\tau_0}\right)^2\right\}. \quad (6)$$

After propagation through the fiber, the pulse is broadened and chirped, with a width

$$\tau_1 = \frac{1}{\tau_0} \times [\tau_0^4 + (\beta_2 L_f)^2]^{1/2} \quad (7)$$

and a frequency-domain representation of

$$E_{out}^f(\omega) = \sqrt{2\pi}\tau_0 \exp\{-j\beta_0 L_f\} \exp\{-j\beta_1 L_f(\omega - \omega_0)\} \times \exp\{-\frac{1}{2}(\tau^2 + j\beta_2 L_f)(\omega - \omega_0)^2\}. \quad (8)$$

We next transmit the broadened pulse through a uniform Bragg grating with coupling coefficient κ , Bragg resonant

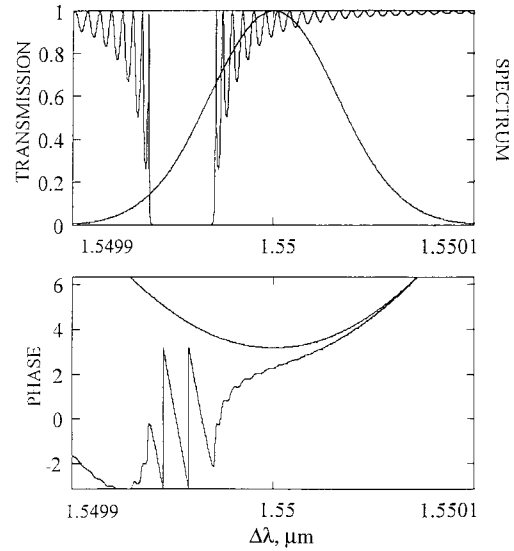


Fig. 6. The grating transmission magnitude and the input pulse spectrum (upper plot), and the phase for the dispersion-broadened pulse and for the transmitted pulse (lower plot).

angular frequency ω_B , and length L_g . Coupled-mode theory provides the result for amplitude transmission in the frequency domain [9]

$$E_{out}^g(\omega) = \sqrt{2\pi}\tau_0 \exp\{-j\phi_0\} \exp\{-j\phi_1\omega\} \times \frac{\gamma \exp\{-\frac{1}{2}\omega^2(\tau^2 + j\beta_2 L_f)\}}{\gamma \cos(\gamma L_g) - j\frac{n}{c}(\omega + \Omega) \sin(\gamma L_g)} \quad (9)$$

where

$$\phi_0 = \beta_0 L_f + \frac{nL_g \Omega}{c}$$

$$\phi_1 = \beta_1 L_f + \frac{nL_g}{c}$$

$$\gamma = \sqrt{\left[\frac{n}{c}(\omega + \Omega)\right]^2 - \kappa^2}$$

and we have defined $\Omega = \omega_0 - \omega_B$ to be the detuning of the central optical frequency from the resonant frequency and redefined ω to be the deviation from the center optical frequency ($\omega - \omega_0 \rightarrow \omega$).

We observe that all dispersion information is contained in the last term of (9), as the group velocity dispersion arises from the second frequency derivative of the phase. In Fig. 6, we plot the grating transmission magnitude and the input pulse spectrum for a typical near-optimum case. The mechanism for pulse compression may be seen in the second curve of Fig. 6 where we plot the phase $\phi(\lambda)$ for the incident dispersion-broadened pulse and for the transmitted field using (9). We see that the grating performs two functions. First, the strong dispersion of the grating tends to flatten the phase curvature over a region of maximum transmission. Second, some truncation of the pulse occurs at frequencies where the grating dispersion would add to the fiber dispersion.

Again, we have performed two-parameter optimizations for this grating geometry, varying the detuning parameter Ω , the grating coupling strength κ , and the grating length L_g . In Fig. 7, we fix $\kappa = 0.19\pi \text{ cm}^{-1}$ and plot the compression

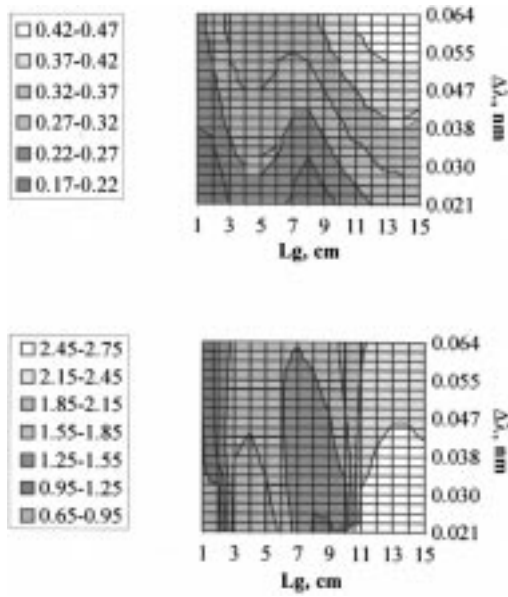


Fig. 7. The peak intensity and compression ratio as functions of the detuning $\Delta\lambda$ and the length of the grating L_g , with a fixed coupling coefficient $\kappa = 0.19\pi \text{ cm}^{-1}$.

(τ_1/τ_2) and peak intensity versus Ω and L_g . (Note that compression is again defined as FWHM ratio.) We observe peak compressions exceeding 2.4, with intensity transmission of approximately 0.44 (compared with the dispersed pulse intensity of 0.28, normalized to the initial, undispersed pulse.)

We see a periodicity with grating length, and although compression does not appear to be strongly sensitive to detuning, the pulse intensity improves with detuning. The compression data may be misleading, however, as zero detuning indicates that the central frequencies of the pulse are mostly reflected by the grating, so the transmitted intensity is small. The curve shows the general tendency that longer grating lengths and large detuning (in the regions shown) provide best performance. Increasing detuning much beyond the interval shown will reduce the compression toward unity, however.

Fig. 8 shows the dependence of our measures on coupling strength and detuning for fixed grating length (14 cm). We see a much stronger periodicity with κ , and again the intensity increases with detuning, while compression does not appear to depend strongly on detuning. Pulse shape is the best indicator for desired operating conditions. Although the pulse shape cannot be well quantified for display on this type of graph, we observe general improvement (e.g., lower sidelobe levels, more Gaussian shape) with increasing coupling strength.

For completeness, we have included Fig. 9, which uses a fixed detuning of 0.05 nm, plotting compression and intensity versus κ and L_g . Here regions of optimum performance are quite clear, with periodicity observed in κ , as we might expect. We see that the dependence on L_g is weak upon reaching a threshold length around 10 cm.

In Fig. 9, we have labeled two regions of optimum performance on subsequent peaks. Point *A*, with parameters ($\kappa = 0.314 \text{ cm}^{-1}$ and $L_g = 10 \text{ cm}$), achieves compression of 2.16 and intensity of 0.416. Point *B* has parameters ($\kappa = 0.565 \text{ cm}^{-1}$ and $L_g = 15 \text{ cm}$), achieving compression of 2.42

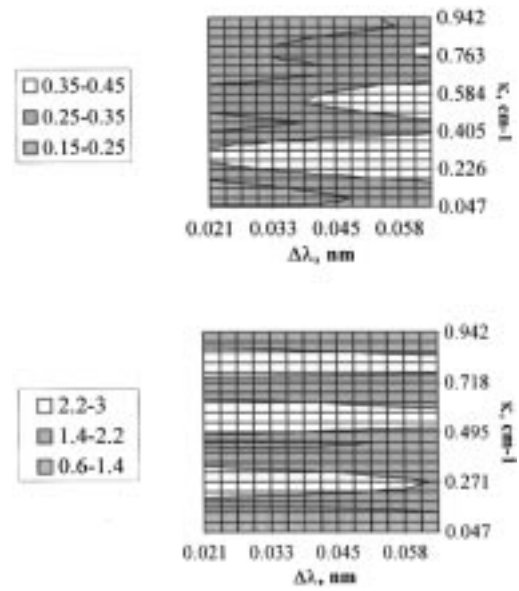


Fig. 8. The peak intensity and compression ratio as functions of the detuning $\Delta\lambda$ and the coupling strength κ , with the grating length L_g fixed at 14 cm.

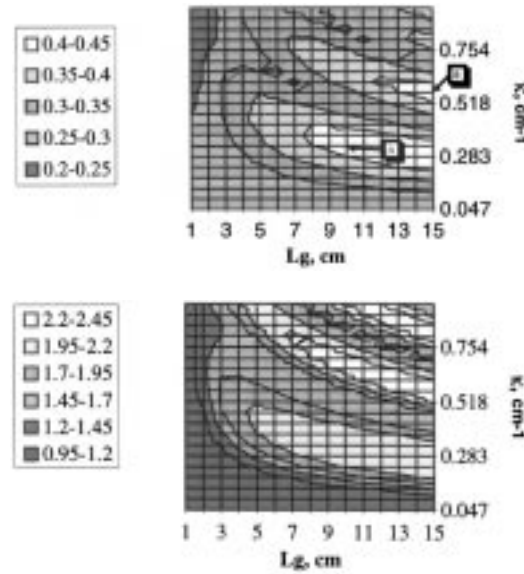


Fig. 9. The peak intensity and compression ratio as functions of the grating length L_g and the coupling strength κ , with a fixed detuning of 0.05 nm.

and intensity 0.421. Plots of the transmitted pulses in these cases are shown in Fig. 10, along with the input dispersed pulse. We observe that the shape of *B* is slightly better, with lower sidelobe levels and improved compression.

IV. CONCLUSIONS

We conclude with a brief summary of the significance of our results. First, we have performed an extensive optimization/sensitivity analysis for chirped, reflective Bragg grating dispersion compensators. Our results for optimum performance agree well with the distributed reflection analysis of [2]. Our results also show that nearly perfect compensation (in our case, compression of 3.60) is achievable with these reflective systems. We have also shown that the tapered grating allows

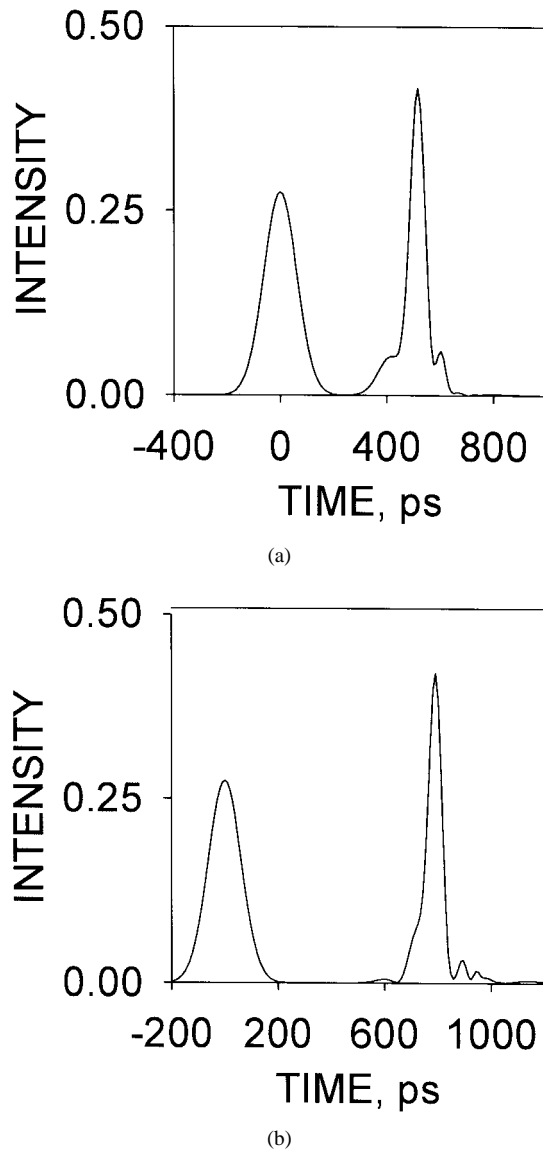


Fig. 10. The transmitted pulse profiles for grating parameters (a) ($\kappa = 0.314 \text{ cm}^{-1}$, $L_g = 10 \text{ cm}$, and $\Delta\lambda = 0.05 \text{ nm}$) and (b) ($\kappa = 0.565 \text{ cm}^{-1}$, $L_g = 15 \text{ cm}$, and $\Delta\lambda = 0.05 \text{ nm}$), along with the dispersion-broadened pulse profile.

reduced sensitivity of compensator performance to variations in coupling strength. This has relevance to point-by-point grating fabrication systems, where writing-beam intensity variations may induce local changes in coupling coefficient κ . In addition, the index-lowering effects of annealing hydrogen-loaded fiber gratings will have greater effect on untapered gratings than on tapered gratings.

Second, we have introduced a new transmission geometry for grating compensators using weak, uniform gratings of only moderate lengths. By detuning the uniform grating center frequency with respect to the center frequency of the optical pulse, pulse compression ratios of over 2.4 have been obtained in the examples shown, with peak intensities of exceeding 0.4.

For the parameter ranges considered in our example, complete compensation was not achievable, largely due to the restriction on grating strength and length. In addition, the

trailing structure in the transmitted pulse is indicative of the presence of cubic and higher order dispersion in the grating transmission spectrum in the sidelobe region of the reflection peak. As we show in a second paper in this issue, complete compensation may be obtained by employing much stronger coupling coefficients and longer grating lengths [11].

Transmission-based compensators have several potential advantages over the reflective systems. The gratings could be written in-line during fabrication of the fiber itself. In addition, the insertion loss of about 4 dB in our example compares relatively well with the reflective systems; with optimized grating systems, this loss can be reduced to fractions of a decibel. In reflective systems, directional couplers or optical circulators must be employed in a two-pass geometry, introducing insertion losses on the order of 6 dB or 2–3 dB, respectively, and increasing the cost per compensator significantly. Thus, the transmission-based system may be a viable, low-cost alternative to reflective systems.

REFERENCES

- [1] D. K. W. Lam, B. K. Garside, and K. O. Hill, "Dispersion cancellation using optical-fiber filters," *Opt. Lett.*, vol. 7, no. 6, pp. 291–293, 1982.
- [2] F. Ouellette, "Dispersion cancellation using linearly chirped Bragg grating filters in optical waveguides," *Opt. Lett.*, vol. 12, pp. 847–849, 1987.
- [3] F. Ouellette, J.-F. Cliche, and S. Gagnon, "All-fiber devices for chromatic dispersion compensation based on chirped distributed resonant coupling," *J. Lightwave Technol.*, vol. 12, pp. 1728–1738, 1994.
- [4] K. O. Hill, S. Theriault, B. Malo, T. Bilodeau, T. Kitagawa, D. C. Johnson, J. Albert, K. Takiguchi, T. Kataoka, and K. Hagimoto, "Chirped in-fiber Bragg grating dispersion compensators: Linearization of dispersion characteristics and demonstration of dispersion compensation in 100 km, 10 Gbit/s optical fiber link," *Electron. Lett.*, vol. 30, pp. 1755–1756, 1994.
- [5] B. J. Eggleton, P. A. Krug, L. Poladian, K. A. Ahmed, and H. F. Lui, "Experimental demonstration of compression of dispersed optical pulses by reflection from self-chirped optical fiber Bragg gratings," *Opt. Lett.*, vol. 19, pp. 877–879, 1994.
- [6] W. H. Loh, R. I. Laming, X. Gu, M. N. Zervas, M. J. Cole, T. Widdowson, and A. D. Ellis, "10-cm chirped fiber Bragg grating for dispersion compensation at 10 Gbit/s over 400 km of nondispersion-shifted fiber," *Electron. Lett.*, vol. 31, pp. 2203–2204, 1995.
- [7] W. H. Loh, R. I. Laming, N. Robinson, A. Cavacinti, F. Vaninetti, C. J. Anderson, M. N. Zervas, and M. J. Cole, "Dispersion compensation over distances in excess of 500 km for 10-Gb/s systems using chirped fiber gratings," *IEEE Photon. Technol. Lett.*, vol. 8, no. 7, pp. 944–946, 1996.
- [8] S. Thibault, J. Lauzon, J.-F. Cliche, J. Martin, M. A. Duguay, and M. Tetu, "Numerical analysis of the optimal length and profile of a linearly chirped fiber Bragg grating for dispersion compensation," *Opt. Lett.*, vol. 20, pp. 647–649, 1995.
- [9] F. Ouellette, "Limits of chirped pulse compression with an unchirped Bragg grating filter," *Appl. Opt.*, vol. 29, no. 32, pp. 4826–4829, 1990.
- [10] B. J. Eggleton, T. Stephens, P. A. Krug, G. Dhosi, Z. Brodzeli, and F. Ouellette, *Electron. Lett.*, vol. 32, p. 1610, 1990.
- [11] N. L. Litchinitser, B. J. Eggleton, and D. B. Patterson, "Fiber Bragg gratings for dispersion compensation in transmission: Theoretical model and design criteria for nearly ideal pulse recompression," *J. Lightwave Technol.*, see this issue, pp. 1303–1313.
- [12] H. Kogelnik, "Filter response of nonuniform almost periodic structures," *Bell Syst. Tech. J.*, vol. 55, pp. 109–127, 1976.

Natalia M. Litchinitser, for a biography, see this issue, p. 1313.

David B. Patterson (M'93) for a biography, see this issue, p. 1313.